Distribution Agreement

In presenting this thesis as a partial fulfillment of the requirements for a degree from Emory University, I hereby grant to Emory University and its agents the non-exclusive license to archive, make accessible, and display my thesis in whole or in part in all forms of media, now or hereafter now, including display on the World Wide Web. I understand that I may select some access restrictions as part of the online submission of this thesis. I retain all ownership rights to the copyright of the thesis. I also retain the right to use in future works (such as articles or books) all or part of this thesis.

Ryan McCann April 13, 2020

Development of Region-Specific Tau Pathology in P301S Mice

by

Ryan McCann

David Weinshenker, PhD
Adviser

Department of Neuroscience and Behavioral Biology

David Weinshenker, PhD
Adviser

Lary Walker, PhD
Committee Member

Dieter Jaeger, PhD
Committee Member

Claire Galloway, PhD
Committee Member

2020

Development of Region-Specific Tau Pathology in P301S Mice

By

Ryan McCann

David Weinshenker, PhD
Adviser

An abstract of
a thesis submitted to the Faculty of Emory College of Arts and Sciences
of Emory University in partial fulfillment
of the requirements of the degree of
Bachelor of Science with Honors

Neuroscience and Behavioral Biology

2020

Abstract
Development of Region-Specific Tau Pathology in P301S Mice
By Ryan McCann

Alzheimer's disease (AD) is a common neurodegenerative disease that is characterized by two main pathologies: the aggregation of tau protein into neurofibrillary tangles (NFT) and the aggregation of amyloid precursor protein fragments into amyloid-β (Aβ) plaques. This project focuses on tau pathology, which is more strongly correlated with the neurodegeneration and cognitive impairment in AD. In humans, tau pathology can first be detected in a vulnerable brainstem region, the noradrenergic locus coeruleus (LC), before appearing in the forebrain later in disease progression. The goal of this project was to determine whether this time-dependent pattern of tau pathology is recapitulated in the P301S transgenic mouse, a popular rodent model of AD-like tauopathy that overexpresses an aggregation-prone mutant form of human tau. The transgene promoter used to produce these mice (mouse prion promoter) is expressed simultaneously in the brainstem and forebrain, suggesting that tau pathology may develop in all neurons at a similar time. However, due to several intrinsic vulnerabilities of LC neurons, we hypothesized that tau pathology would first develop in the LC, and then in downstream memory regions such as entorhinal cortex (EC) and hippocampus (HC). To determine the order of pathology development in each brain region in P301S mice, we used immunofluorescence to detect hyperphosphorylated tau, an early form of pathology, at 1-2, 3-4, 5-6 and 7-8 months of age. We found that the first brain region to show a significant level of tau pathology compared to wild-type control was the CA3 region of the HC (1-2 months), followed by the LC and dentate gyrus region of the HC (3-4) months, the EC (5-6 months), and finally the CA1 region of the HC (7-8 months). Thus, while there was selective region vulnerability in P301S mice, they did not demonstrate the progression of tau pathology seen in human AD.

Development of Region-Specific Tau Pathology in P301S Mice

By

Ryan McCann

David Weinshenker, PhD
Adviser

A thesis submitted to the Faculty of Emory College of Arts and Sciences
of Emory University in partial fulfillment
of the requirements of the degree of
Bachelor of Science with Honors

Neuroscience and Behavioral Biology

2020

Acknowledgements

Thank you to everyone in the Weinshenker laboratory for their help learning techniques used in this project:
David Weinshenker, PhD
Jason Schroeder, PhD
Claire Galloway, PhD
Cannan Jerome
Rachel Pearcy-Tillage
Stephanie Foster
Danny Lustberg
Alexa Iannitelli
Michael Kelberman
Shivaang Chawla
Genevieve Wilson
Andy Chen

Thank you to my committee members for their advice and assistance on this project:
David Weinshenker, PhD
Dieter Jaeger, PhD
Lary Walker, PhD
Claire Galloway, PhD

Thank you to Seong Su Kang of the Ye laboratory for providing the N368 antibody for the pilot.

Table of Contents

Figures and Tables

Introduction

Alzheimer's Disease (AD) is a neurodegenerative disease resulting from the aggregation of misfolded proteins. AD leads to the impairment of thought, memory, and language, and is the 6th leading cause of death in the United States (1, 2). AD is identified post mortem by the aggregation of tau protein into intracellular neurofibrillary tangles (NFT) and amyloid-β (Aβ) protein into extracellular plaques (1). Aggregated forms of these proteins can lead to loss of neuronal function and eventual cell death, resulting in brain atrophy and worsening of AD symptoms over time (1). In the quest to vanquish this disease, AD-like pathology is often studied in laboratories using transgenic rodents because normal mice and rats do not develop plaques or NFTs (3, 4). One tau-based transgenic model is the P301S (B6N.Cg-Tg(Prnp-MAPT*P301S)PS19Vle/J) tau transgenic mouse (5). The goal of this project was to determine if this mouse model accurately recapitulates the progression of tau pathology seen in human AD.

Under healthy conditions, tau protein acts in the formation and stabilization of axonal microtubules (6). In AD and several other neurodegenerative diseases, tau becomes hyperphosphorylated, which leads to misfolding, aggregation, and the formation of NFTs (7). Hyperphosphorylated tau is currently the earliest detectable AD-like pathology in the human brain (1, 7). There are both soluble and insoluble forms of hyperphosphorylated tau that are toxic, resulting in the destruction of microtubules, disruption of axonal transport, and neuronal dysfunction (7, 8). Hyperphosphorylated tau has prion-like properties that allow it to spread between neurons and brain regions (1, 9, 10). Once hyperphosphorylated, tau polymerizes into paired helical filaments (PHFs), and subsequently aggregates into NFTs (6). Given this progression, early regions expressing tau pathology may hold the key to understanding the origins of AD and its progression. Tau pathology is correlated with cognitive decline and neurodegeneration (11, 12). In comparison, amyloid pathology does not correlate well with these

aspects of AD and thus is not a strong indicator of the disease state (12). These relationships suggest that studies of tau pathology are of extreme importance to understanding the development and progression of AD.

Recent studies indicate that aberrant tau can be detected in the human locus coeruleus (LC), the major noradrenergic nucleus of the brain as early as the first few decades of life (1). Hyperphosphorylated tau is present in the LC of 72% of subjects aged 31-40 years, and 94% of subjects in the 41- to 50-year age group (13). Because the incidence of LC tau pathology is higher than the incidence of AD, it stands to reason that other factors are needed to transform this initial form of pathology into the full-fledged disease (14). Nevertheless, the LC has recently become a focal point of AD research for several reasons. First, the LC is the earliest known location of hyperphosphorylated tau in the human brain (1). Second, the LC innervates and is the sole source of norepinephrine (NE) in most of the forebrain, including the hippocampus (HC) and the entorhinal cortex (EC) – brain regions vital to learning and memory that are affected in AD (15, 16). Third, LC dysfunction has been implicated in aspects of prodromal AD, including disruption of normal sleep patterns, anxiety, depression, and agitation (17). Finally, the LC degenerates in later disease (18), and LC integrity appears to encode cognitive reserve in the face of forebrain pathology (19).

Ideally, the specific effects of pathogenic tau could be studied in model animals, particularly in animals that mimic the progression of tau pathology from the LC to the forebrain such as that is observed in human AD. For the purpose of this project, the EC and HC have been selected because they are directly innervated by the LC and also develop tau pathology at a relatively early stage (particularly the EC, albeit later than the LC) (20). The HC is comprised of several sub-regions: the dentate gyrus (DG), CA3, CA2, and CA1 (21). This project will focus on the DG, CA3, and CA1. The EC projects to the DG, which then connects to CA3, which

projects to CA1 (21). In AD, the levels of tau pathology can vary between these sub-regions (14).

One limitation of using mice in AD research is that endogenous mouse tau is resistant to aggregation, necessitating the surgical seeding of preformed tau fibrils or transgenic expression of pathogenic tau for studying AD in this species (3, 4). The P301S mouse is a popular model of tau pathology, with a search for "P301S mouse" on PubMed yielding over 1200 publications within the last 10 years. This transgenic mouse overexpresses a mutant form of human tau that is prone to both hyperphosphorylation and aggregation and causes frontotemporal dementia (FTD) (5). Although this mutation causes FTD but not AD in humans, it produces toxic forms of tau reminiscent of those found in AD. It has been reported that hyperphosphorylated tau begins appearing in the HC of P301S mice at 3 months of age. By 6 months, PHFs (the more advanced form of filamentous tau) are evident and neuronal loss can be detected in the forebrain at 8 months (5). However, because the appearance and progression of tau pathology in the LC has not been reported for young mice it is unclear whether the P301S mouse is a good model for the stereotypical pattern of pathology in human AD.

The transgene used to create the P301S mouse includes the mouse prion (Prnp) promoter, which in theory drives expression of mutant human tau simultaneously in most neurons (5). Thus, it would be reasonable to assume that all P301S expressing neurons would begin to show pathology at the same time. However, the development of tau pathology might be accelerated in LC neurons owing to several factors. Due to its location close to both blood vessels and the fourth ventricle, the LC is continuously exposed to environmental toxins (17). The axons of the LC are thin and unmyelinated, and the constant pacemaker activity of the LC can produce oxidative stress, increasing the LC's vulnerabilities to pathology (17). Additionally, the NE that is produced in the LC is broken down into toxic metabolites, specifically 3,4-

dihydroxyphenylglycolaldehyde (DOPEGAL). DOPEGAL activates asparagine endopeptidase (AEP), which cleaves tau at position N368 and produces a truncated form that is more prone to hyperphosphorylation, aggregation, and toxicity than the full-length protein (22). In that study, it was reported that hyperphosphorylated tau (AT8+) staining appeared at 3 months in the LC of the P301S mice, but they did not examine younger mice or compare brain regions (22). The combination of environmental exposure, neuronal morphology, pacemaker activity, and toxic metabolites create a perfect storm for the development of tau pathology in the LC.

The P301S mice have been examined in a multitude of ways. The Weinshenker laboratory most recently used them to examine the effects on forebrain tau pathology when the LC is ablated using a noradrenergic-selective neurotoxin (3). These animals experienced accelerated tau load and cell death in the HC, demonstrating that NE and the LC play a role in the development of tau pathology. There is data to suggest that tau pathology may develop early in the LC of young P301S mice. That experiment determined that proteopathic tau seeding, a predictor of tau pathology, can be detected in the brainstem at 1.5 months (23). The LC is located in the brainstem, so the presence of this marker could suggest early development of pathology in the LC (23). Tau seeding is mentioned in the brainstem, but IHC staining for hyperphosphorylated tau was only performed in the HC and cortex, leaving a lack of information pertaining to LC-specific tau pathology in young P301S mice (23). Young mice may demonstrate vulnerability to tau pathology in the P301S model due to the aggressive nature of pathology development, which is usually lethal by 9-10 months (24).

Based on the evidence described above, we expected that tau pathology in P301S mice would appear first in the LC before forebrain regions. In spite of the prion promoter driving tau development across the brain, we predicted that the pattern of pathology in the mice would mimic what is seen in human AD, first developing in the LC, and then later appearing in the EC

and HC. Due to the nature of the promoter used in these mice, it cannot be deduced if the pathogenic tau in these mice is spread through a prion-like method versus produced endogenously by any given neuron, but it is possible to determine where the hyperphosphorylated tau first appears. In this study, we used immunohistochemical staining to analyze the pathology in the LC, EC, and HC at multiple ages to determine the time course of tau pathology development between regions important in AD.

Hypothesis

Due to the intrinsic vulnerabilities of the LC, we hypothesized that the tau pathology would develop in the LC before the EC and HC.

Methods

Animals

The project used LC, EC, and HC tissue from 1-2, 3-4, 5-6, and 7-8 month-old male and female P301S (B6N.Cg-Tg(Prnp-MAPT*P301S)PS19Vle/J) tau transgenic mice, and wild-type littermate controls (2 from each age group).

Perfusion and Tissue Collection

Mice were injected with pentobarbital and transcardially perfused with 0.1x KPBS followed by 4% PFA. Following brain extraction, brains were drop-fixed in 4% PFA overnight, and then moved to 30% sucrose. 40 micron thick sections were collected using a Leica cryostat. Brain regions were determined using a mouse brain atlas (25).

Antibodies

An antibody against tyrosine hydroxylase (TH) (Abcam ab76442) was used to mark noradrenergic neurons of the LC. A mouse anti-AT8 (Thermofisher MN1020) antibody was used to detect an early form of hyperphosphorylated tau. A pilot study was also performed with a rabbit anti-N368 tau antibody (Millipore ABN1703), which detects an asparagine endopeptidase-

cleaved form of highly toxic tau (22). Secondary antibodies used were goat anti chicken 488 (Abcam ab150169), goat anti mouse 568 (Thermofisher A-11004), and goat anti rabbit 568 (Thermofisher A-11011). DAPI counterstaining was used to identify the neuronal subdivisions of the HC.

Free Floating Section Fluorescent Staining

Brain slices were placed in a solution of sodium citrate for 3 min at 90° C to retrieve antigens. Slices were allowed to cool and were then placed in a blocking solution of 2% normal goat serum (NGS) and 1% bovine serum albumin (BSA) in PBST for 30 min. The slices were then washed in PBS. Primary antibodies were diluted in PBST, 1% NGS, and 0.5% BSA and slices were incubated overnight at 4° C. The following day, slices were washed in PBS, and then incubated for 2 h in secondary antibody diluted in PBST, 1% NGS, and 0.5% BSA. Following incubation in secondary, the slices were washed in PBS, then mounted with mounting media, and coverslipped with fluoromount containing DAPI.

Imaging

Slides were viewed under a Leica DM6000B epifluorescent microscope. Images were taken at 10x and 20x of the LC, and 5x, 10x, and 20x of the EC, and the HC.

Analysis

Images were analyzed using the ImageJ software. Values for immunoreactivity (IR) were determined in ImageJ by uniformly thresholding all images, and taking the mean gray value from the LC as marked by TH neurons, or a subsection region of interest (ROI) for the DG, CA1, CA3, and EC. Each ROI was defined for one specific brain region. All data was collected from 20x images of each brain region. Following collection of data, the experimenter was unblinded, and data were normalized to the controls. Data were analyzed by a one-way ANOVA followed by Tukey's multiple comparisons tests, where appropriate, using GraphPad PRISM 8.

Results

AT8 Pathology in the Locus Coeruleus

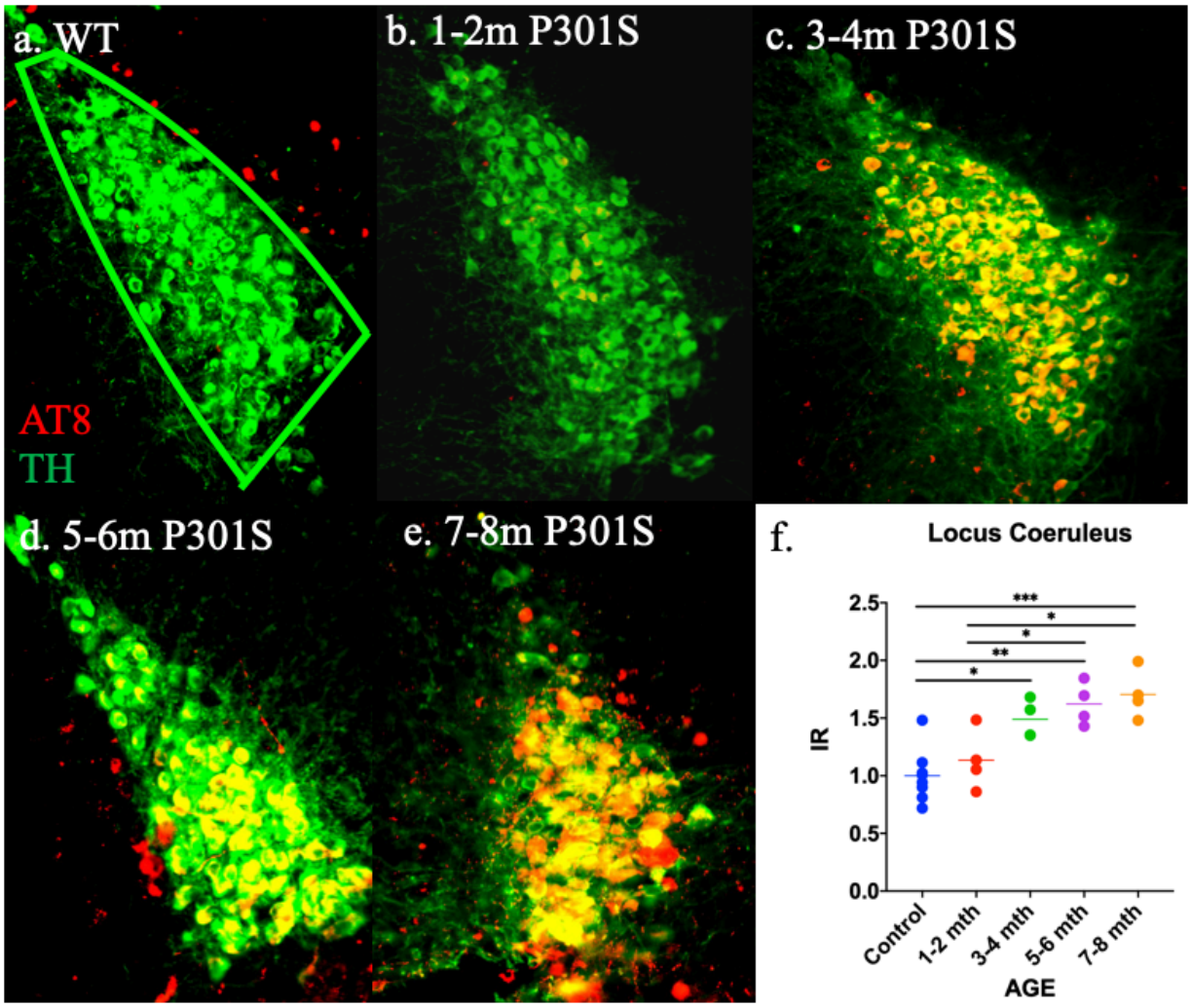

Figure 1. AT8 IR in the LC of P301S mice. A: Representative image of 7-8 month old WT LC with ROI used on Image J shown. B-E: Shown are representative images of the LC in P301S mice. (Red = AT8, Green = TH) F: Quantification of IR in the LC for WT and each age group. ns- P>.05, *- P≤ 0.05, **- P≤ 0.01, ***- P≤ 0.001, ****- P≤ 0.0001. Significance bars represent significance seen in post-hoc analysis.

In the LC, one-way ANOVA revealed a significant effect of age ($F_{4, 19}$=10.75, p=0.0001), and post hoc tests showed that the level of AT8 IR was first significantly different from the wild-type controls at 3-4 months (q=5.201, p=0.0122) and was also higher at all subsequent ages (5-6 months: q=6.609, p=0.0014; 7-8 months: q=7.497, p=0.0004). Within the P301S group, there

was a significant difference between the 1-2 month group and both the 5-6 month (q=4.488, p=0.0356) and 7-8 month mice (q=5.257, p=0.0112) (Figure 1).

AT8 Pathology in the Entorhinal Cortex

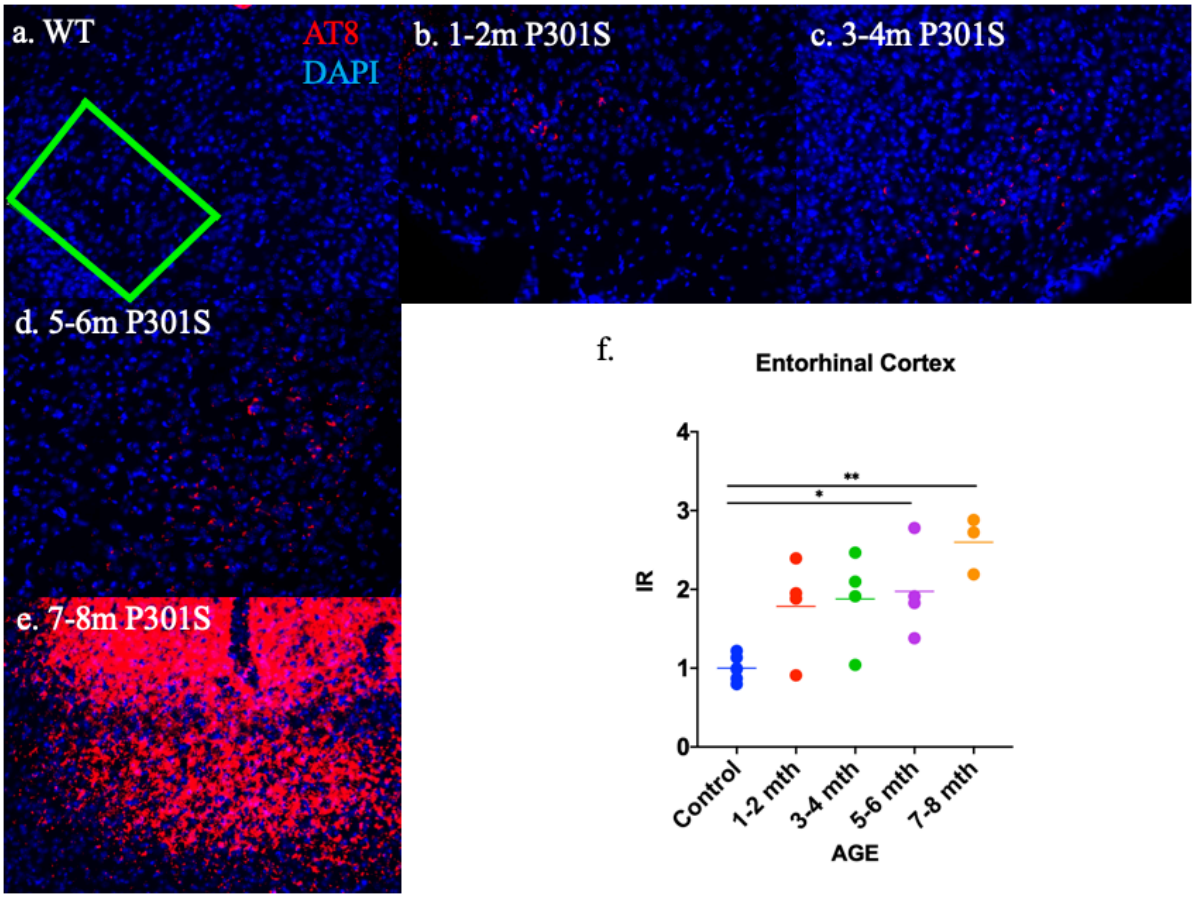

Figure 2. AT8 IR in the EC of P301S mice. A: Representative image of 7-8 month old WT EC with ROI used on Image J shown. B-E: Shown are representative images of the EC in P301S mice. (Red = AT8, Blue = DAPI. F: Quantification of IR in the EC for WT and each age group. ns- P>.05, *- P≤ 0.05, **- P≤ 0.01, ***- P≤ 0.001, ****- P≤ 0.0001. Significance bars represent significance seen in post-hoc analysis.

In the EC, one-way ANOVA revealed a significant effect of age ($F_{4, 16=}$ 6.296, p=0.0031), and post hoc tests showed that the level of AT8 immunoreactivity (IR) was first significantly different from the wild-type controls at 5-6 months (q=4.449, p=0.0427) and was also higher at 7-8 months (q=6.661, p=0.0019). However, the majority of subjects in both the 1-2 and 3-4 month groups did contain AT8 IR but did not reach significance due to one subject with a low

value in each age group. There was no significant change in AT8 IR within P301S age groups (Figure 2).

AT8 Pathology in the CA3 Region of the Hippocampus

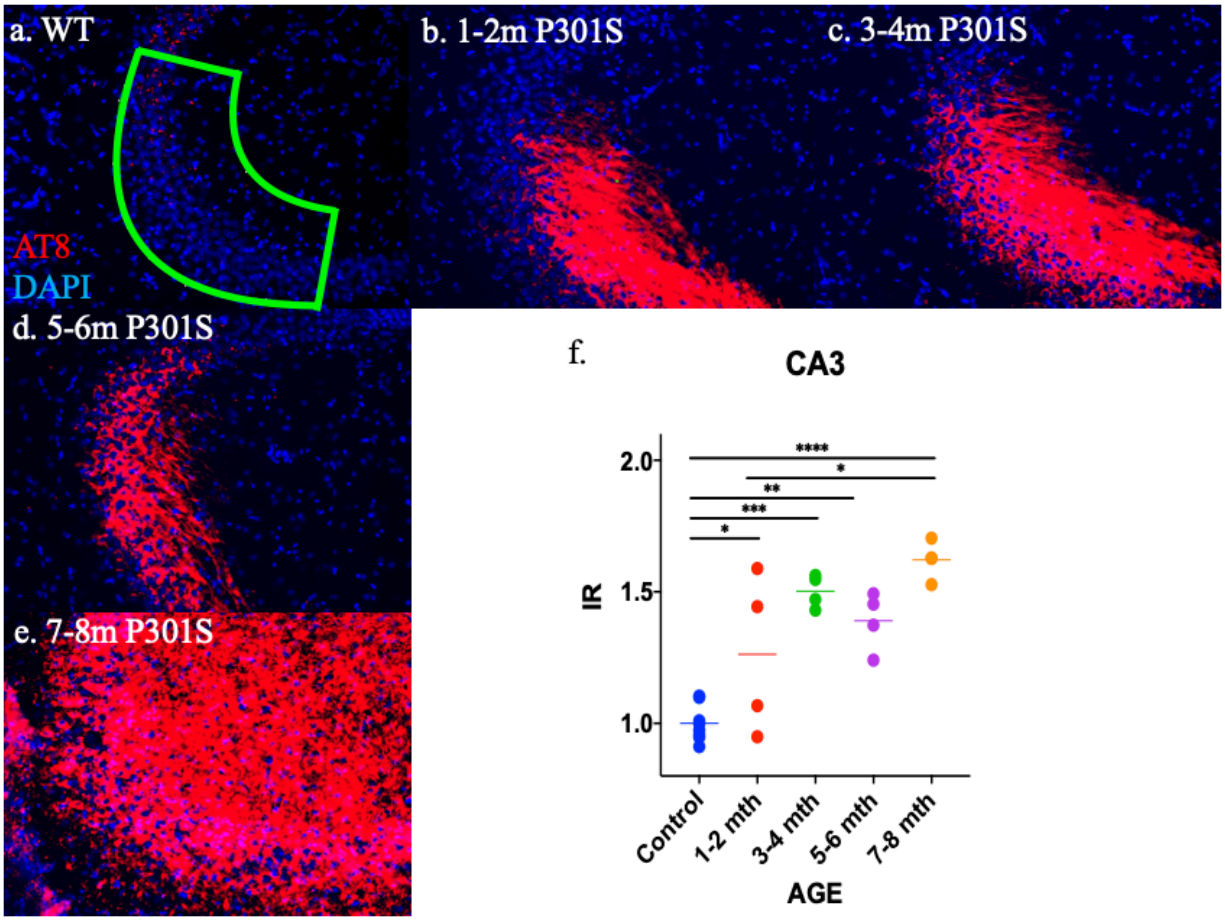

Figure 3. AT8 IR in the CA3 of P301S mice. A: Representative image of 7-8 month old WT CA3 with ROI used on Image J shown. B-E: Shown are representative images of the CA3 in P301S mice. (Red = AT8, Blue = DAPI). F: Quantification of IR in the CA3 for WT and each age group. ns- P>.05, *- P≤ 0.05, **- P≤ 0.01, ***- P≤ 0.001, ****- P≤ 0.0001. Significance bars represent significance seen in post-hoc analysis.

In CA3, one-way ANOVA revealed a significant effect of age ($F_{4, 19=}$ 16.96, $p<0.0001$), and post hoc tests showed that the level of AT8 immunoreactivity (IR) was first significantly different from the wild-type controls at 1-2 months ($q=4.313$, $p=0.0459$) and was also higher in all subsequent age groups (3-4 months: $q=8.272$, $p=0.0001$; 5-6 months: $q=6.417$, $p=0.0019$; 7-8 months: $q=10.23$, $p<0.0001$). It was noted that there were high levels of variance in the 1-2

month group, with two animals similar to WT controls and two animals that had elevated levels of IR. Within the P301S mice, the only significant increase in pathology was between the 1-2 month group and the 7-8 month group (q=5.126, p=0.0137) (Figure 3).

AT8 Pathology in the CA1 Region of the Hippocampus

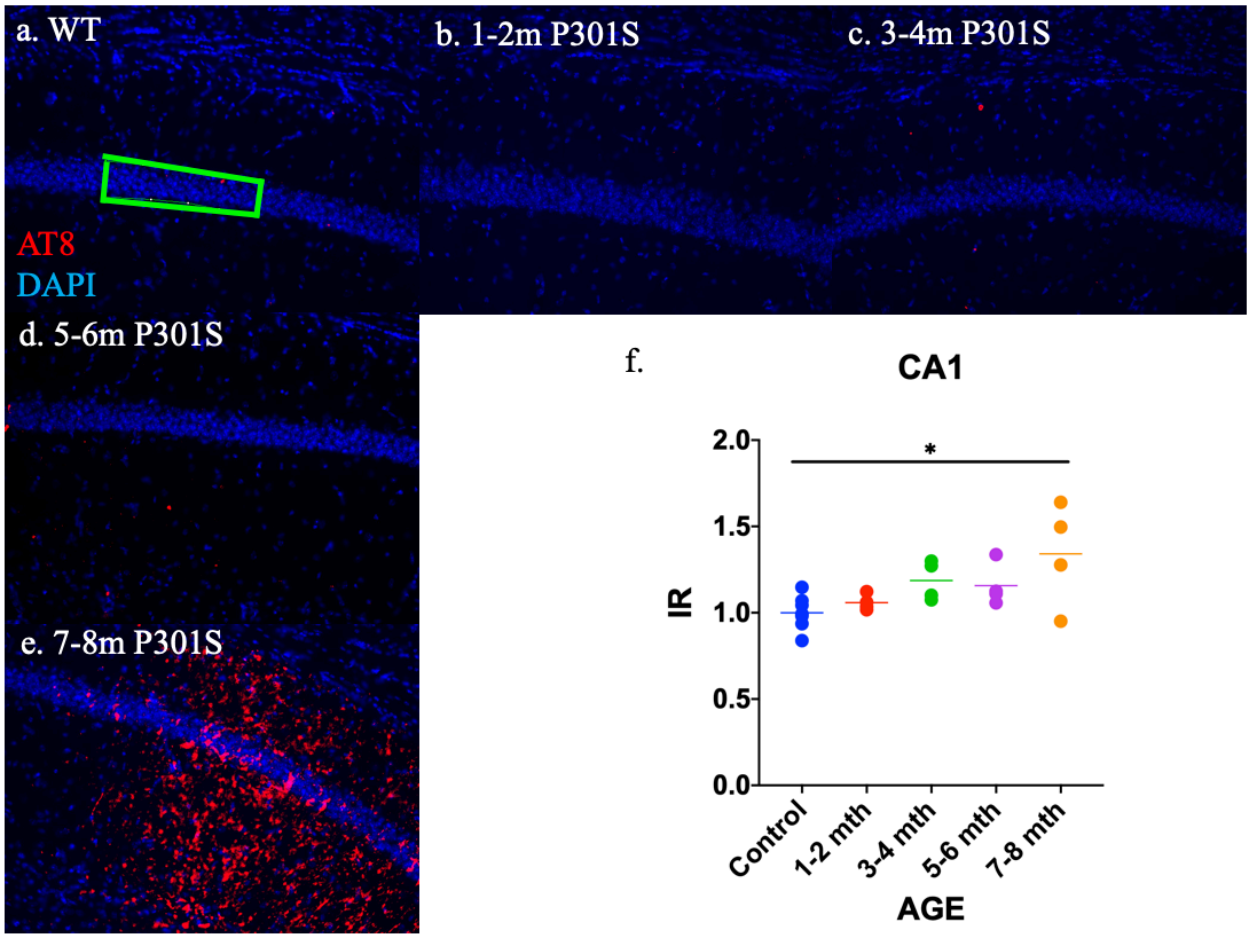

Figure 4. AT8 IR in the CA1 of P301S mice. A: Representative image of 7-8 month old WT CA1 with ROI used on Image J shown. B-E: Shown are representative images of the CA1 in P301S mice. (Red = AT8, Blue = DAPI). F: Quantification of IR in the CA1 for WT and each age group. ns- P>.05, *- P≤ 0.05, **- P≤ 0.01, ***- P≤ 0.001, ****- P≤ 0.0001. Significance bars represent significance seen in post-hoc analysis.

In CA1, one-way ANOVA revealed a significant effect of age ($F_{4, 19}$=3.941, p= 0.0171), and post hoc tests showed that the level of AT8 immunoreactivity (IR) was only significantly different from the wild-type controls at 7-8 months (q=5.296, p=0.0106). There were no significant differences in AT8 IR between any age of the P301S mice (Figure 4).

AT8 Pathology in the Dentate Gyrus of the Hippocampus

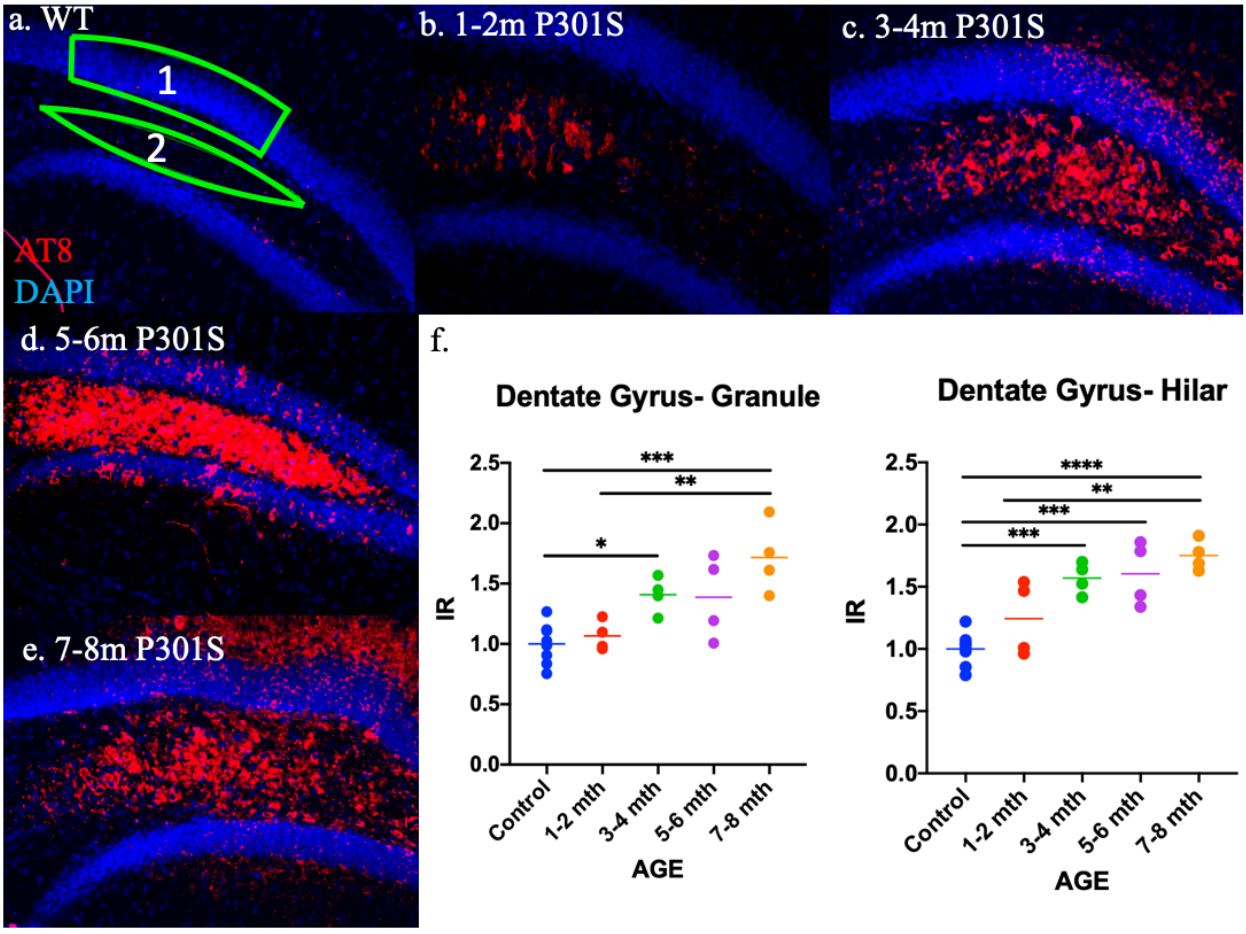

Figure 5. AT8 IR in the DG of P301S mice. A: Representative image of 7-8 month old WT DG with ROIs used (1- Granule, 2- Hilar) on Image J shown. B-E: Shown are representative images of the DG in P301S mice. (Red = AT8, Blue = DAPI). F: Quantification of IR in the DG for WT and each age group. ns- P>.05, *- P≤ 0.05, **- P≤ 0.01, ***- P≤ 0.001, ****- P≤ 0.0001. Significance bars represent significance seen in post-hoc analysis.

We subdivided analysis of DG pathology between the granule cell blades of the DG (Figure 5A.1) and the mossy fiber hilar cells (Figure 5A.2). In both the granule cells ($F_{4, 19}$=8.695, p=0.0004) and the hilar cells ($F_{4, 19}$=14.72, p<0.0001), one-way ANOVA revealed a significant effect of age. In the granule cells, post hoc tests showed the level of AT8 IR first was significantly different from WT controls at 3-4 months (q=4.292, p=0.0473), then was nominally significant at 5-6 months (q=4.079, p=0.0639), and significant at 7-8 months (q=7.534, p=0.0003). There is a significant difference in AT8 IR between the 1-2 month P301S group and

the 7-8 month P301S group (q=5.922, p=0.0040). Post hoc tests revealed that the hilar neurons first significantly differed from WT controls at 3-4 months (q=6.939, p=0.0008) and at all subsequent age groups (5-6 months: q=5.838, p=0.0046; 7-8 months: q=8.203, p=0.0001). Within the P301S animals, the only significant increase in pathology was between the 1-2 month group and the 7-8 month group (q=5.341, p=0.0099).

AT8 Pathology Progression Between Brain Regions

AT8 IR Compared to Control								
Brain Region	1-2 month		3-4 month		5-6 month		7-8 month	
CA3	1.262	*	1.503	***	1.390	**	1.622	****
LC	1.134	ns	1.489	*	1.622	**	1.705	***
DG- Granule	1.066	ns	1.408	*	1.387	ns	1.716	***
DG- Hilar	1.244	ns	1.570	***	1.604	***	1.751	****
EC	1.784	ns	1.879	ns	1.974	*	2.598	**
CA1	1.059	ns	1.187	ns	1.157	ns	1.341	*

Table 1. AT8 pathology IR in P301S mice as compared to control (control = 1.000). The means and significance are displayed and sorted by brain region and age. ns- P>.05, *- P≤ 0.05, **- P≤ 0.01, ***- P≤ 0.001, ****- P≤ 0.0001.

We next examined the data to determine the order of tau pathology appearance. A region was considered having developed pathology when it's AT8 IR was significantly different from the WT control animals. The first region to demonstrate significant pathology was the CA3 of the HC, which showed significance in the 1-2 month animals. At 3-4 months, the LC demonstrated significant amounts of AT8 IR over WT followed by the EC at 5-6 months and CA1 at 7-8 months. The DG showed different pathology within its sub-regions, with the dense granule blades showing significant difference from control at 3-4 months, and then not at 5-6 months. In the hilar mossy fiber cells of the DG, significance of AT8 IR was seen at the 3-4 month age group, and significance was maintained through the age groups (Table 1 and Figure 6).

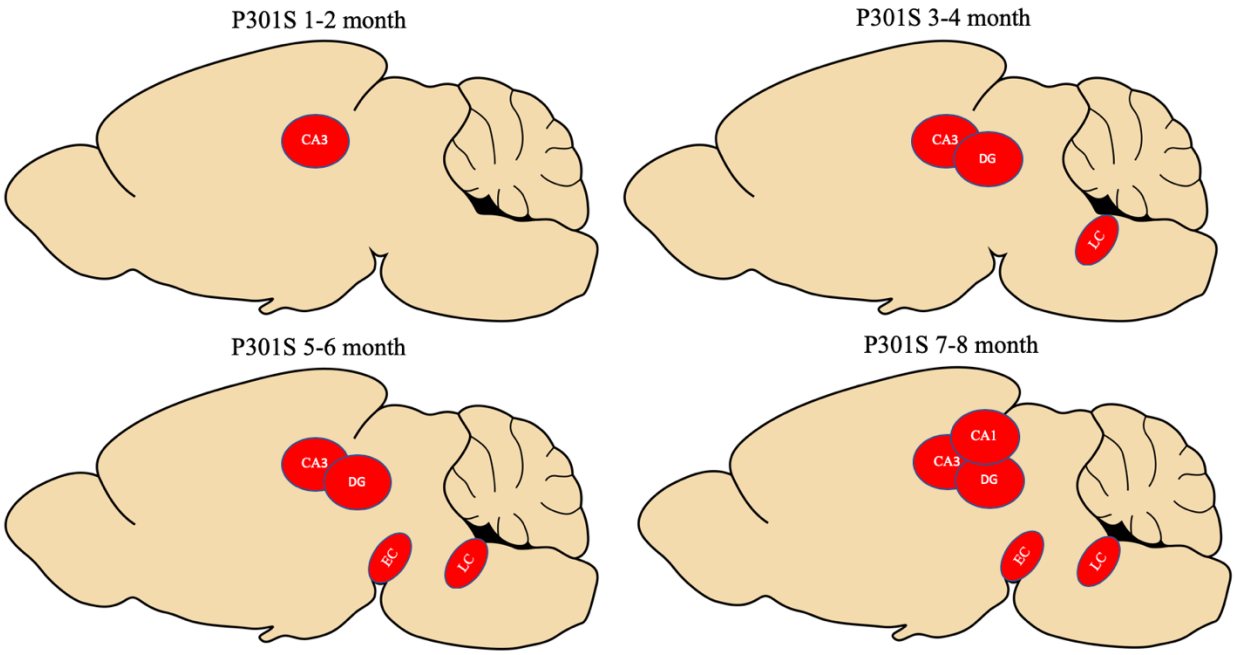

Figure 6. Representation of regions displaying AT8 IR significance from WT control in the mouse brain at different ages. Red circle corresponds to a positive region.

N 368 Cleaved Tau

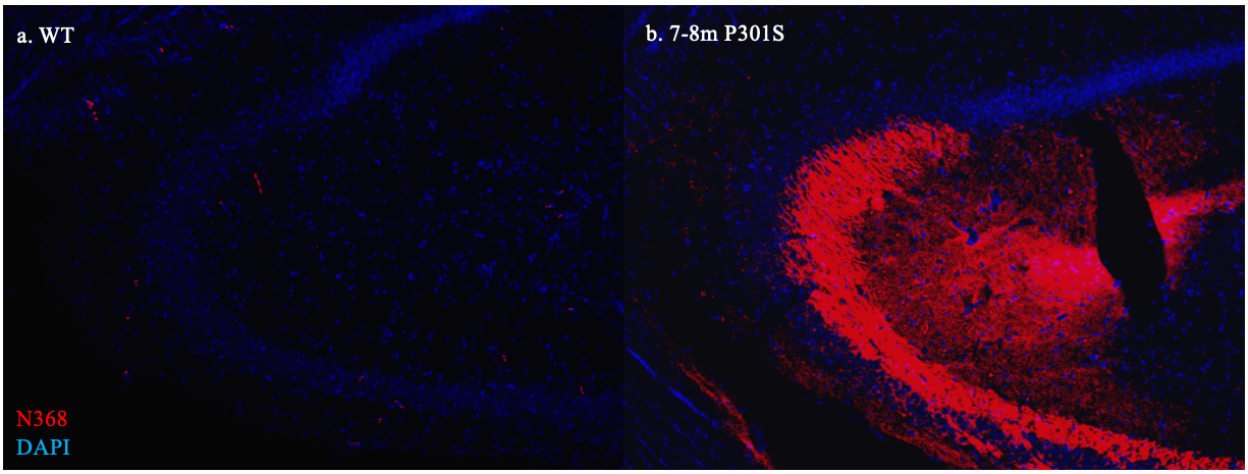

Figure 7. N368 IR in the CA2 and CA3 of P301S mice. A: Shown is the HC of a WT mouse. B: Shown is the HC of a 7-8 month old P301S mouse. (Red = N368, Blue = DAPI).

We conducted a pilot experiment in the hippocampal region of one 7-8 month old wild-type mouse and one 7-8 month P301S mouse using an antibody against N368 AEP-cleaved tau to examine the feasibility of examining other forms of pathogenic tau. There was a stark

difference between genotypes, with intense N368 IR exclusively in CA2 and CA3 from the P301S subject (Figure 7).

Discussion

A major limitation of this study was the low N and high variability of pathology within a given brain region. Sufficiently powering this study would likely provide a more accurate picture of tau pathology development of tau pathology in the P301S mice. In this case, the statistical analyses may be misleading, for example in the EC where 3/4 P301S subjects showed higher AT8 IR than WT controls at 1-2 months, but a single subject with low AT8 IR rendered the group difference non-significant. A power calculation revealed that at least N=5 would be required to detect significance with a $p<0.05$ and 80% power. This is just the most obvious example, but there were several others where more subjects would increase confidence in the conclusions. Further restricting the age groups (e.g. separating 1 month and 2 month animals from the 1-2 month group) would not make an appreciable difference because there was no correlation between age within a group and AT8 IR intensity (data not shown). Thus, due to the underpowered nature of this project, all subsequent interpretation and discussion of the data using the statistics come with this caveat.

Because the progression of pathology did not fit the pattern seen in AD, we wondered if it might be more reminiscent of human FTD, given that the P301S mutation is derived from a FTD patient. Unfortunately, there is not currently a defined progression of tau pathology associated with FTD as there is for AD, particularly for the early stages (26), there is even variability among the few rare individuals with the P301S mutation. For example, in one family, two patients had the same P301S mutation and presented two different types of neurodegeneration, one with FTD and one with corticobasal degeneration (27). Given the lack of

a clear regionally specific spread in FTD, analysis of pathology progression in these mice is limited to comparisons with AD.

Although the data did not support our hypothesis that the LC would develop pathology before the other brain regions analyzed, we did find selective vulnerability of specific brain regions to tau pathology. We demonstrated that the CA3 region of the HC was the first to show significant levels of pathology (Table 1). The overall progression did not recapitulate the human AD condition of tau pathology starting in the LC, next appearing in the EC, and finally the HC (20). The LC did developed pathology relatively early (3-4 months) but was preceded by AT8 development in CA3 (1-2 months). Additionally, the EC showed strong levels of pathology in both the 1-2 and 3-4 month groups, but in each group, there was one animal with a low level of AT8 IR, which drove non-significance (Figure 2). These data suggests that while the LC is more vulnerable than some other regions, in this particular model, the CA3 and EC appear to be more susceptible. In human AD, of HC sub-regions, the CA1 experiences the most significant loss of neurons, notably more than the CA3 (28). It is important to note, however, that the development of AT8 pathology does not necessarily correlate linearly with quicker onset of cell death (13), so though CA3 may be vulnerable to developing tau pathology earlier, the neurons of the CA1 may die at a younger age.

The data from the HC are consistent with AT8 pathology as measured in previous reports by the Weinshenker laboratory and others. Those experiments, using DAB instead of immunofluorescence, showed higher AT8 pathology at younger ages in CA3 compared to CA1 and the DG (3). In the original paper discussing the creation of the P301S mice, it was noted that the mossy fibers in the CA3 region develop tau pathology at a relatively young age (5). The CA3 seems to be a region susceptible to tau pathology. In AD, it has been shown that the mossy fibers of the CA3 stratum lucidum layer, which is a region of strong connectivity to the DG, shows

high levels of AT8 pathology, even when corresponding DG granule bodies do not (29). These mossy fibers also appear to be accumulating early pathology in the P301S mice, as the shape of the CA3 stratum lucidum mirrors what is seen in CA3 AT8 IR (Figure 3 B-F), even without a significant presence of AT8 in the granule cells. Mossy fibers of the DG also show vulnerability to AD-like pathology other than hyperphosphorylated tau. A recent study using a transgenic mouse expressing mutant amyloid precursor protein (APP) and presenilin 1 (PS1) genes found that the synapses of mossy fibers projecting to CA3 from the granule cells of the DG were altered at a young age (30). The early effect on these axons in both the P301S and APP/PS1 mouse models, expressing different AD-like pathology, further suggests that these axons may be particularly susceptible in AD. Additionally in the HC, DG hilar neurons show early and strong pathology (Figure 5F). The hilar neurons are vulnerable in temporal lobe epilepsy, but their role in AD is unclear (31). Amyloid is associated with abnormal neuronal hyperactivity, with epilepsy comorbid in 10-22% of AD patients (32), and the hilar neurons appear to be vulnerable in both disease states. (30). Another intrahippocampal projection pathway, from CA3 to the CA1 stratum radiatum, demonstrates AD pathology in humans, even while CA3 cell bodies did not (29). In our study, axons from CA3 to CA1 did not seem to follow this pattern, even when CA3 cell bodies were AT8+ (Figure 3, 4). Further experimentation should be performed to determine whether advanced tau pathology seen in the HC of P301S mice follows the human AD pattern of affecting axons before the cell bodies. Axons are more vulnerable to tau pathology, and generally degenerate before neuronal death (33, 34). This may explain why the connective pathways demonstrate higher AT8 IR than the cell bodies.

Interestingly, the level of pathology seen in CA3 and the DG hilar cells appear to be related. In the 1-2 month age group, both regions demonstrated variable AT8 IR. Two animals were above control in each group, and two were at the level of control (Figure 3F, 5F). The data

shows the animals were consistent in their relationship of AT8 IR level for both regions, meaning if they were high IR in CA3, they had high IR in the hilar cells. This may indicate some sort of relationship between pathology in the two regions and could be further studied in these mice at a young age.

The EC, though not statistically significant in the 1-2 or 3-4 month old groups, showed early pathology in 3/4 of the P301S mice (Figure 2). The lateral EC (LEC), which we targeted for quantification, is a region that is extremely susceptible to tau pathology in AD (35, 36). It was proposed that higher metabolism in the LEC leads to its greater vulnerability to pathology in AD (36). This vulnerability can explain why the EC appears to develop tau early on and may perhaps explain the variability seen as well. It is possible that sections where the aberrant tau load was lower originated in the more resilient medial EC (MEC) (36). EC tissue was very fragile, and tore easily, making it difficult to determine the exact anatomical location of each slice.

In general, AT8 levels appeared to be relatively stable once they initially developed (Figures 1F, 2F, 3F, 4F, 5F). The only significant increases within P301S mice seen were in the LC (between the 1-2 month group and both the 5-6 month and 7-8 month group; Figure 1F) and CA3 (between the 1-2 month group and the 7-8 month group; Figure 3F). These results suggest that once AT8 pathology begins developing within a brain region, it accumulates very rapidly, then settles at a “steady state”, possibly as more advanced forms of pathogenic tau develop.

In the future, this project should be expanded to analyze the tissue using different antibodies that detect various forms of aberrant tau. The pilot experiment with the N368 antibody against AEP-cleaved tau showed strong staining in both CA2 and CA3 of 8-month-old P301S mice (Images 26, 27). Further analysis can be performed to detect the presence of AEP-cleaved tau in the LC and other brain regions across all age groups. Additionally, an antibody against

PHF tau, a more advanced form of pathology, can be used to analyze the severity of tau pathology within brain regions. Though PHF1 staining first appears in the HC of P301S mice around 6 months of age (5), it may appear earlier in the LC or EC. Staining using thioflavin S can also be performed. Thioflavin S binds to β-sheets that accumulate in bona fide NFTs. These stains can be used to determine if other forms of tau follow a similar pattern as AT8 pathology, with regards to brain region progression as well as rapid development followed by steady state levels. It has been reported that thioflavin S staining first appears after 9 months in the P301S mice (23), but this analysis was not performed in the LC, where pathology may progress more rapidly. Additional IHC staining can be performed for astrocytic (GFAP) and microglial (IBA1) neuroinflammation, another hallmark of AD that may influence tau pathology and cell death (37).

Overall, the data collected from P301S mice suggest that they can be very useful for investigating general mechanisms of tau pathology and cell death, but not for studying the mechanisms underlying the stereotypical progression seen in human AD.

References

1. Chalermpalanupap T, Weinshenker D, Rorabaugh JM. Down but Not Out: The Consequences of Pretangle Tau in the Locus Coeruleus. Neural Plast. 2017;2017:7829507.
2. Heron M. Deaths: Leading Causes for 2016. Natl Vital Stat Rep. 2018;67(6):1-77.
3. Chalermpalanupap T, Schroeder JP, Rorabaugh JM, Liles LC, Lah JJ, Levey AI, et al. Locus Coeruleus Ablation Exacerbates Cognitive Deficits, Neuropathology, and Lethality in P301S Tau Transgenic Mice. J Neurosci. 2018;38(1):74-92.
4. Clavaguera F, Bolmont T, Crowther RA, Abramowski D, Frank S, Probst A, et al. Transmission and spreading of tauopathy in transgenic mouse brain. Nat Cell Biol. 2009;11(7):909-13.
5. Yoshiyama Y, Higuchi M, Zhang B, Huang SM, Iwata N, Saido TC, et al. Synapse loss and microglial activation precede tangles in a P301S tauopathy mouse model. Neuron. 2007;53(3):337-51.
6. Iqbal K, Liu F, Gong CX, Grundke-Iqbal I. Tau in Alzheimer disease and related tauopathies. Curr Alzheimer Res. 2010;7(8):656-64.
7. Braak H, Del Tredici K. Where, when, and in what form does sporadic Alzheimer's disease begin? Curr Opin Neurol. 2012;25(6):708-14.
8. Kopeikina KJ, Hyman BT, Spires-Jones TL. Soluble forms of tau are toxic in Alzheimer's disease. Transl Neurosci. 2012;3(3):223-33.
9. de Calignon A, Polydoro M, Suarez-Calvet M, William C, Adamowicz DH, Kopeikina KJ, et al. Propagation of tau pathology in a model of early Alzheimer's disease. Neuron. 2012;73(4):685-97.
10. Iba M, McBride JD, Guo JL, Zhang B, Trojanowski JQ, Lee VM. Tau pathology spread in PS19 tau transgenic mice following locus coeruleus (LC) injections of synthetic tau fibrils is determined by the LC's afferent and efferent connections. Acta Neuropathol. 2015;130(3):349-62.
11. Buerger K, Ewers M, Andreasen N, Zinkowski R, Ishiguro K, Vanmechelen E, et al. Phosphorylated tau predicts rate of cognitive decline in MCI subjects: a comparative CSF study. Neurology. 2005;65(9):1502-3.
12. Small GW, Siddarth P, Kepe V, Ercoli LM, Burggren AC, Bookheimer SY, et al. Prediction of cognitive decline by positron emission tomography of brain amyloid and tau. Arch Neurol. 2012;69(2):215-22.
13. Braak H, Thal DR, Ghebremedhin E, Del Tredici K. Stages of the pathologic process in Alzheimer disease: age categories from 1 to 100 years. J Neuropathol Exp Neurol. 2011;70(11):960-9.
14. Llorens-Martin M, Blazquez-Llorca L, Benavides-Piccione R, Rabano A, Hernandez F, Avila J, et al. Selective alterations of neurons and circuits related to early memory loss in Alzheimer's disease. Front Neuroanat. 2014;8:38.
15. Benarroch EE. The locus ceruleus norepinephrine system: functional organization and potential clinical significance. Neurology. 2009;73(20):1699-704.
16. Jacobs HIL, Hedden T, Schultz AP, Sepulcre J, Perea RD, Amariglio RE, et al. Structural tract alterations predict downstream tau accumulation in amyloid-positive older individuals. Nat Neurosci. 2018;21(3):424-31.
17. Weinshenker D. Long Road to Ruin: Noradrenergic Dysfunction in Neurodegenerative Disease. Trends Neurosci. 2018;41(4):211-23.

18. Kelly SC, He B, Perez SE, Ginsberg SD, Mufson EJ, Counts SE. Locus coeruleus cellular and molecular pathology during the progression of Alzheimer's disease. Acta Neuropathol Commun. 2017;5(1):8.
19. Wilson RS, Nag S, Boyle PA, Hizel LP, Yu L, Buchman AS, et al. Neural reserve, neuronal density in the locus ceruleus, and cognitive decline. Neurology. 2013;80(13):1202-8.
20. Braak H, Del Tredici K. Alzheimer's pathogenesis: is there neuron-to-neuron propagation? Acta Neuropathol. 2011;121(5):589-95.
21. Setti SE, Hunsberger HC, Reed MN. Alterations in Hippocampal Activity and Alzheimer's Disease. Transl Issues Psychol Sci. 2017;3(4):348-56.
22. Kang SS, Liu X, Ahn EH, Xiang J, Manfredsson FP, Yang X, et al. Norepinephrine metabolite DOPEGAL activates AEP and pathological Tau aggregation in locus coeruleus. J Clin Invest. 2020;130(1):422-37.
23. Holmes BB, Furman JL, Mahan TE, Yamasaki TR, Mirbaha H, Eades WC, et al. Proteopathic tau seeding predicts tauopathy in vivo. Proc Natl Acad Sci U S A. 2014;111(41):E4376-85.
24. Hovakimyan A, Antonyan T, Shabestari SK, Svystun O, Chailyan G, Coburn MA, et al. A MultiTEP platform-based epitope vaccine targeting the phosphatase activating domain (PAD) of tau: therapeutic efficacy in PS19 mice. Sci Rep. 2019;9(1):15455.
25. Paxinos G, Franklin KBJ. The mouse brain in stereotaxic coordinates. Compact 2nd ed. Amsterdam ; Boston: Elsevier Academic Press; 2004.
26. Bodea LG, Eckert A, Ittner LM, Piguet O, Gotz J. Tau physiology and pathomechanisms in frontotemporal lobar degeneration. J Neurochem. 2016;138 Suppl 1:71-94.
27. Bugiani O, Murrell JR, Giaccone G, Hasegawa M, Ghigo G, Tabaton M, et al. Frontotemporal dementia and corticobasal degeneration in a family with a P301S mutation in tau. J Neuropathol Exp Neurol. 1999;58(6):667-77.
28. Padurariu M, Ciobica A, Mavroudis I, Fotiou D, Baloyannis S. Hippocampal neuronal loss in the CA1 and CA3 areas of Alzheimer's disease patients. Psychiatr Danub. 2012;24(2):152-8.
29. Christensen KR, Beach TG, Serrano GE, Kanaan NM. Pathogenic tau modifications occur in axons before the somatodendritic compartment in mossy fiber and Schaffer collateral pathways. Acta Neuropathol Commun. 2019;7(1):29.
30. Viana da Silva S, Zhang P, Haberl MG, Labrousse V, Grosjean N, Blanchet C, et al. Hippocampal Mossy Fibers Synapses in CA3 Pyramidal Cells Are Altered at an Early Stage in a Mouse Model of Alzheimer's Disease. J Neurosci. 2019;39(21):4193-205.
31. Scharfman HE, Myers CE. Hilar mossy cells of the dentate gyrus: a historical perspective. Front Neural Circuits. 2012;6:106.
32. Miranda DDC, Brucki SMD. Epilepsy in patients with Alzheimer's disease: A systematic review. Dement Neuropsychol. 2014;8(1):66-71.
33. Kneynsberg A, Combs B, Christensen K, Morfini G, Kanaan NM. Axonal Degeneration in Tauopathies: Disease Relevance and Underlying Mechanisms. Front Neurosci. 2017;11:572.
34. Braak H, Del Tredici K. The pathological process underlying Alzheimer's disease in individuals under thirty. Acta Neuropathol. 2011;121(2):171-81.
35. Adams JN, Maass A, Harrison TM, Baker SL, Jagust WJ. Cortical tau deposition follows patterns of entorhinal functional connectivity in aging. Elife. 2019;8.
36. Khan UA, Liu L, Provenzano FA, Berman DE, Profaci CP, Sloan R, et al. Molecular drivers and cortical spread of lateral entorhinal cortex dysfunction in preclinical Alzheimer's disease. Nat Neurosci. 2014;17(2):304-11.

37. Calsolaro V, Edison P. Neuroinflammation in Alzheimer's disease: Current evidence and future directions. Alzheimers Dement. 2016;12(6):719-32.